Supplementary Information for:

Metallized SU-8 thin film patterns on stretchable PDMS

Tiffany Baëtens, Emiliano Pallecchi, Vincent Thomy, and Steve Arscott

Institut d'Electronique, de Microélectronique et de Nanotechnologie (IEMN), CNRS, The University of Lille, Cité Scientifique, 59652 Villeneuve d'Ascq, France.

1. Shadow and photo masks used for the study

Supplementary Figure S1 shows shadow and photo masks used in the study.

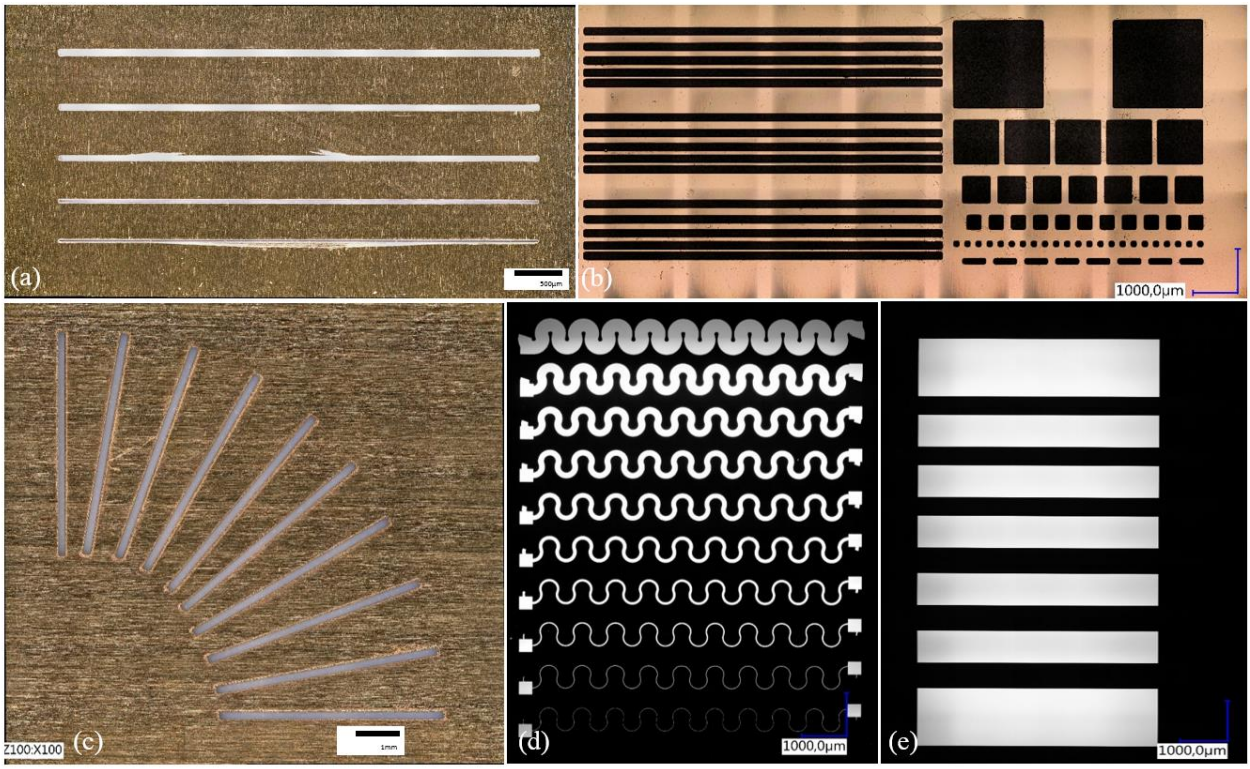

Supplementary Figure S1. Photographs of the shadow masks and photomasks used in the study. (a) 'Mask 1', (b) 'Mask 2', and (c) 'Mask 3' are shadow masks for process 1 described in the article. (d) and (e) are photomasks employed for process 2 described in the article.

2. Samples which resulted in wrinkling of the SU-8 film

2.1 Experimental results

Supplementary Figure S2 shows process-induced wrinkling in the SU-8 skin on PDMS.

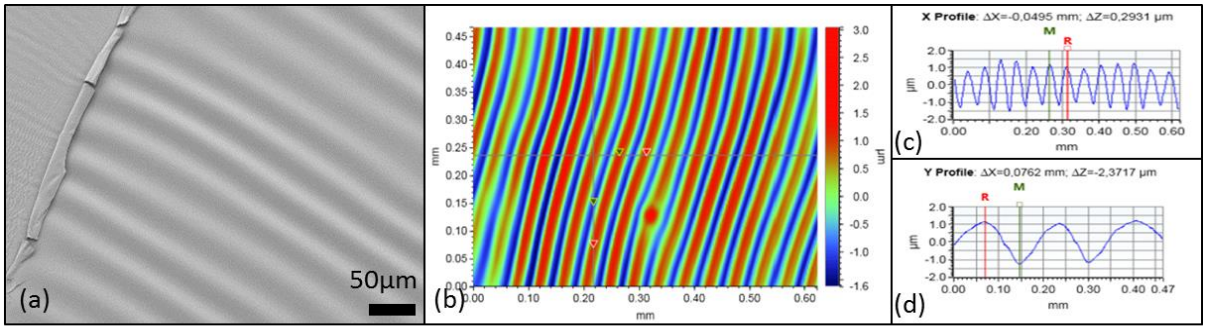

Supplementary Figure S2. Process-induced wrinkling of the SU-8 film on PDMS. (a) Scanning electron microscopy (SEM) image of wrinkles in a lithographically patterned 800 nm thick SU-8 skin on PDMS. (b) Optical interference surface profiler characterization of the wrinkles. (c) and (d) shows profiles of wrinkles. (c) and (d) present the frequency and the amplitude of wrinkles respectively.

Supplementary Figure S2(a) shows a scanning electron microscopy (SEM) image of the wrinkling of the SU-8 skin. This is due to thermally-induced compressive stress. The period and amplitude of the wrinkling was measured using a 3D optical interference surface profiler—see Supplementary Figure S2(b-d). In general, the wrinkling was perpendicular to the longest lengths of the SU-8 lines. The period of the

wrinkling λ was measured to be 49.5 µm and its amplitude was 2.4 µm. This is in contrast to the wrinkling which could be observed in larger surface SU-8 skins—see Supplementary Figure S3—where the wrinkles are more randomly orientated.

2.2 Large area surfaces

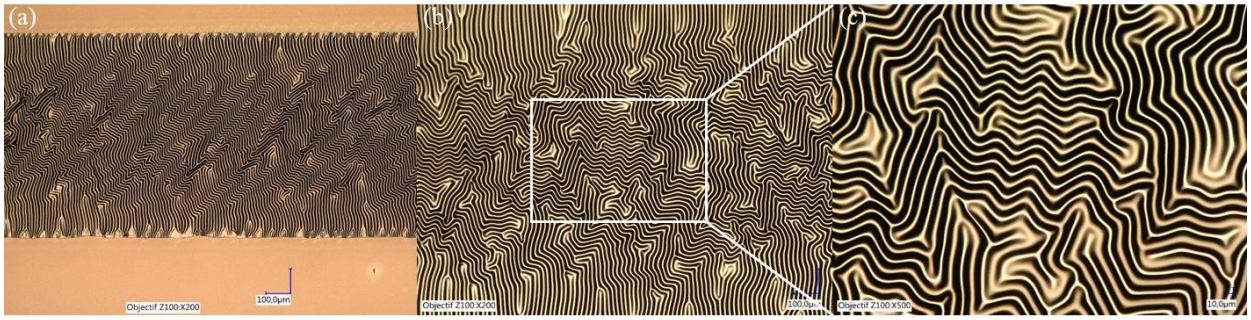

Supplementary Figure S3. Optical microscopy at different zooms (a-c) showing wrinkling of the metallized SU-8 films on PDMS. See scale bars for dimensions.

2.3 Modelling of the wrinkles

In the absence of an externally applied strain the total stress σ_{tot} in the SU-8 film is the intrinsic stress σ_{int} (due to e.g. solvent loss and molecular cross linking during polymerization) plus the extrinsic stress σ_{th} (due to thermal expansion).

The *in plane* extrinsic stress σ_{th} in the SU-8 is given by:

$$\sigma_{th} = \alpha_{SU-8} - \alpha_{PDMS}\frac{E_{SU-8}}{1-\nu_{SU-8}}(T_{PEB} - T_0) \qquad (1)$$

where α_{SU-8} and α_{PDMS} are the *linear* expansion coefficients of the SU-8 and PDMS (remembering that $\alpha_L = CTE/3$), E_{SU-8} and ν_{SU-8} are the elastic modulus and Poisson coefficient of the SU-8, and T_{PEB} and T_0 are the post exposure bake (PEB) and ambient temperatures.

The critical compressive stress σ_{crit} for wrinkling in the SU-8 film is given by:

$$\sigma_{crit} = 0.52\left(\frac{E_{SU-8}}{1-\nu_{SU-8}^2}\right)^{\frac{1}{3}}\left(\frac{E_{PDMS}}{1-\nu_{PDMS}^2}\right)^{\frac{2}{3}} \quad (2)$$

Where E_{PDMS} and ν_{PDMS} are the elastic modulus and Poisson coefficient of the PDMS.

The period of the wrinkles λ_{SU-8} in the SU-8 film is given by:

$$\lambda_{SU-8} = 2\pi t_{SU-8}\left(\frac{E_{SU-8}(1-\nu_{PDMS}^2)}{3E_{PDMS}(1-\nu_{SU-8}^2)}\right)^{\frac{1}{3}} \quad (3)$$

Where t_{SU-8} is the thickness of the SU-8 film.

If we assume that $\sigma_{th} \gg \sigma_{int}$ as the PDMS has a large thermal expansion coefficient then given the physical properties give in the table below, a thickness of SU-8 equal to 800 nm and a PEB = 95°C we can evaluate the in plane stress in the SU-8 to be -64 MPa—i.e. the SU-8 is in compression. The critical compressive stress required for wrinkling of the SU-8 film is computed to be -15.7 MPa. As $\sigma_{crit} < \sigma_{tot}$ wrinkling is predicted having a period λ_{SU-8} of 35.7 µm. This value agrees relatively well with the experimental values given above.

Physical property	**Value**
$\boldsymbol{CTE_{SU-8}}$	5.2×10^{-5} °C^{-1}
$\boldsymbol{CTE_{PDMS}}$	9.6×10^{-4} °C^{-1}

E_{SU-8}	1.7-2.2 GPa
uts_{SU-8}	34-130 MPa
E_{PDMS}	2.6 MPa
ν_{SU-8}	0.22
ν_{PDMS}	0.5
T_{PEB}, T_0	95°C, 20°C

Supplementary Table S1: Physical properties of the SU-8 and the PDMS for the process and conditions used in the study. Mechanical properties of SU-8 [1–4]. Mechanical properties of PDMS [5]. CTE of SU-8 [6]. CTE of PDMS data sheet for Sylgard 184 (Dow Corning, USA).

3. Modelling of the line cracking as the line orientation angle is changed

Supplementary Figure S4 shows an idealized sample containing a single metallized SU-8 line on a PDMS block. The line is orientated at an angle θ relative to the longitudinal direction of the applied global strain (vertical direction on the figure).

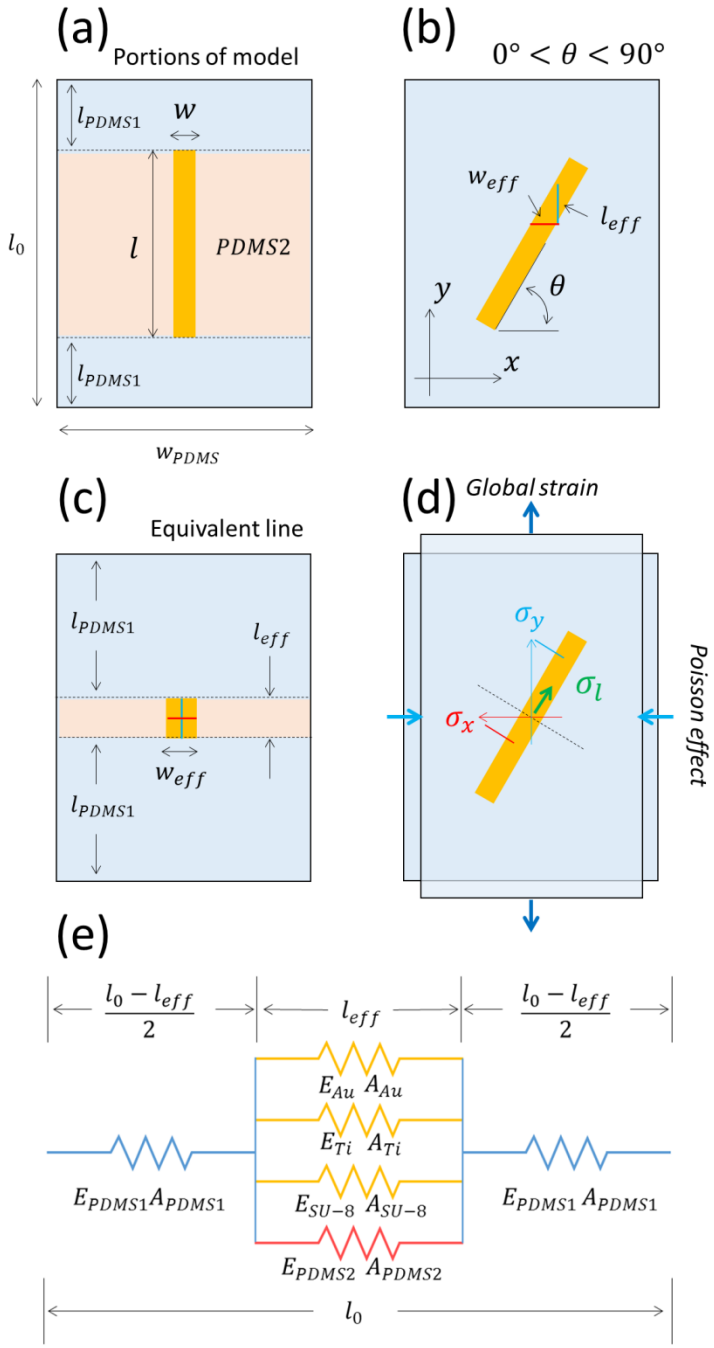

Supplementary Figure S4 Modelling of the metallized SU-8 skin on PDMS. (a) A single thin film Au/Ti/SU-8 line is shown on a thick rectangular PDMS support (light blue). (b) The line is orientated at an angle θ relative to the sample bottom edge. We can define an effective length l_{eff} (blue) and an effective width w_{eff} (red) parallel and perpendicular to the longitudinal direction of the applied strain. (c) The

equivalent straight line to that presented in (b) having dimensions l_{eff} and w_{eff}. (d) Effect of global straining and the associated Poisson effect on the sample. The total *in-line* stress in the line σ_l (green arrow) is given by the difference of the components of σ_x and σ_y projected onto the direction of the line. (e) The Hookean spring-based model of the sample. The model separates the PDMS into three parts: two series PDMS1 portions (light blue) and a PDMS2 portion (light red) which is in parallel with the Au/Ti/SU-8 line (gold).

The sample shown in Supplementary Information Figure S4(a) can be divided up into 3 distinct portions. First, the lines are composed of an Au/Ti/SU-8 thin film multi-layer. The lines have a length l and a width w. For a given orientation angle θ, the line has an effective length l_{eff} and an effective width w_{eff}. The thicknesses of the gold, the titanium, and the SU-8 are t_{Au}, t_{Ti}, and t_{SU-8}. Second, the PDMS portions in series with the lines—these are referred to as PDMS1 (light blue). Third, the PDMS portion in parallel with the lines—this is referred to as PDMS2 (light red). The PDMS block has a length of l_0, a width w_{PDMS}, and a thickness t_{PDMS}. The model assumes a linear-elastic—or Hookean—response to strain, and considers only a single line on the substrate surface.

With reference to Supplementary Figure S4(b), the effective length of the *equivalent straight line* can be approximated by the following formulae:

$$l_{eff} = \frac{w}{\cos\theta} \tag{4}$$

$$w_{eff} = \frac{w}{\sin\theta} \tag{5}$$

The above equations are only valid within certain limits. At angles approaching 90°, if $l_{eff} > l$ then l_{eff} is set to l. At small angles, if $w_{eff} > l$ then w_{eff} is set to l. These dimensions form a sample having an equivalent line shown in to Supplementary Figure S4(c).

Let us first consider the y direction. With reference to Supplementary Figure S4(d), the mechanical strains *in series* (the PDMS1 portions and the effective line/PDMS2 portion) add up to give the total strain:

$$\Delta l_0 = 2\Delta l_{PDMS1} + \Delta l_{eff} \qquad (6)$$

The mechanical forces in the central parallel portion (the line plus the PDMS2 portion) add up to give the total force:

$$F_y = \sigma_y t_{total} = F_{PDMS2} + F_{SU-8} + F_{Ti} + F_{Au} \qquad (7)$$

$$\sigma_y = \frac{1}{t_{total}}(E_{PDMS2}t_{PDMS2} + E_{SU-8}t_{SU-8} + E_{Ti}t_{Ti} + E_{Au}t_{Au})\frac{\Delta l_{eff}}{l_{eff}} \qquad (8)$$

The mechanical strains in parallel are equal:

$$\Delta l_{PDMS2} = \Delta l_{SU-8} = \Delta l_{Ti} = \Delta l_{Au} = \Delta l_{eff} \qquad (9)$$

The sum of the forces in the individual layers of the effective parallel portions (light red and gold in Fig. 7) are equal to the forces in the two series PDMS1 layers—therefore we can write down:

$$\frac{\Delta l_{eff}}{l_{eff}}\sum t_n E_n = t_{PDMS1}E_{PDMS1}\frac{\Delta l_{PDMS1}}{l_{PDMS1}} \qquad (10)$$

The extension in one of the series PDMS1 portions is equal to:

$$\Delta l_{PDMS1} = \frac{\Delta l_0 - \Delta l_{eff}}{2} \qquad (11)$$

Therefore the extension in the line plus PDMS2 portion Δl_{eff} is equal to:

$$\Delta l_{eff} = \frac{\alpha_y}{\alpha_y+\beta_y}\Delta l_0 \quad (12)$$

Where:

$$\alpha_y = \frac{t_{PDMS1}E_{PDMS1}}{2l_{PDMS1}} \quad (13)$$

$$\beta_y = \frac{\sum t_n E_n}{l_{eff}} \quad (14)$$

Therefore the *longitudinal* mechanical stress in the SU-8 layer is given by:

$$\sigma_y^{SU-8} = E_{SU-8}\frac{\Delta l_{eff}}{l_{eff}} \quad (15)$$

Or, in terms for total extension Δl_0:

$$\sigma_y^{SU-8} = \frac{\alpha_y}{(\alpha_y+\beta_y)}\frac{E_{SU-8}}{l_{eff}}\Delta l_0 \quad (16)$$

Let us now consider the x direction. We can use the above arguments to calculate the transversal mechanical stress in the SU-8 line σ_x^{SU-8}. In order to do this, the same equations are used but with modified dimensions where the longitudinal dimensions become the transversal dimensions. We can thus write down an expression for σ_x^{SU-8}:

$$\sigma_x^{SU-8} = \frac{\alpha_x}{(\alpha_x+\beta_x)}\frac{E_{SU-8}}{w_{eff}}\Delta w_0 \quad (17)$$

where:

$$\Delta w_0 \sim \nu_{PDMS}\Delta l_0 \quad (18)$$

We can now calculate the in-line stress σ_l^{SU-8} in the SU-8 *in the direction of the line* which takes into account the orientation angle and the Poisson effect by using the following relationship:

$$\sigma_l^{SU-8} = \sigma_y^{SU-8} \sin\theta - \sigma_x^{SU-8} \cos\theta \qquad (19)$$

These components are indicated in Supplementary Information Figure S4(d). Equations (16), (17), and (18) can now be injected into Equation (19) in order to plot the in-line stress as a function of applied strain $\Delta l_0/l_0$ for various line angles θ.This is shown as a contour plot in Fig. 7 of the article.

It is apparent from Equation (19) that for a given line angle the in-line stress will be zero due to compensation of the applied longitudinal stress by the lateral compressive stress due to the Poisson effect. From Equation (19) if $\sigma_l^{SU-8} = 0$ we have:

$$\tan\theta = \frac{\sigma_x^{SU-8}}{\sigma_y^{SU-8}} \qquad (20)$$

from Equations (15), (16), and (17) we have:

$$\frac{\sigma_x^{SU-8}}{\sigma_y^{SU-8}} \sim \nu_{PDMS} \qquad (21)$$

we have:

$$\theta = \tan^{-1} \upsilon_{PDMS} \qquad (22)$$

4. Applied strain versus average interline strain for the samples tested.

Supplementary Figure S5 shows plots of the average interline strain versus the applied strain. The measurement and calculation of the average interline strain is described in the article.

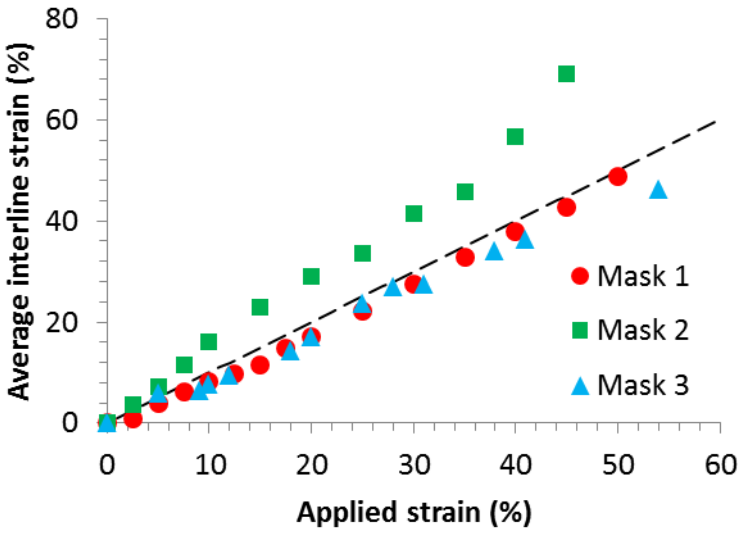

Supplementary Figure S5. Average interline strain plotted as a function of applied strain for 3 types of samples fabricated using 3 types of masking—See Section 1 'Shadow and photo masks used for the study' above. The black dashed line corresponds to a 1:1 plot.

5. Behaviour of metallized SU-8 'horseshoe shaped' lines fabricated using photolithography

5.1 Cracking in horseshoe shaped lines

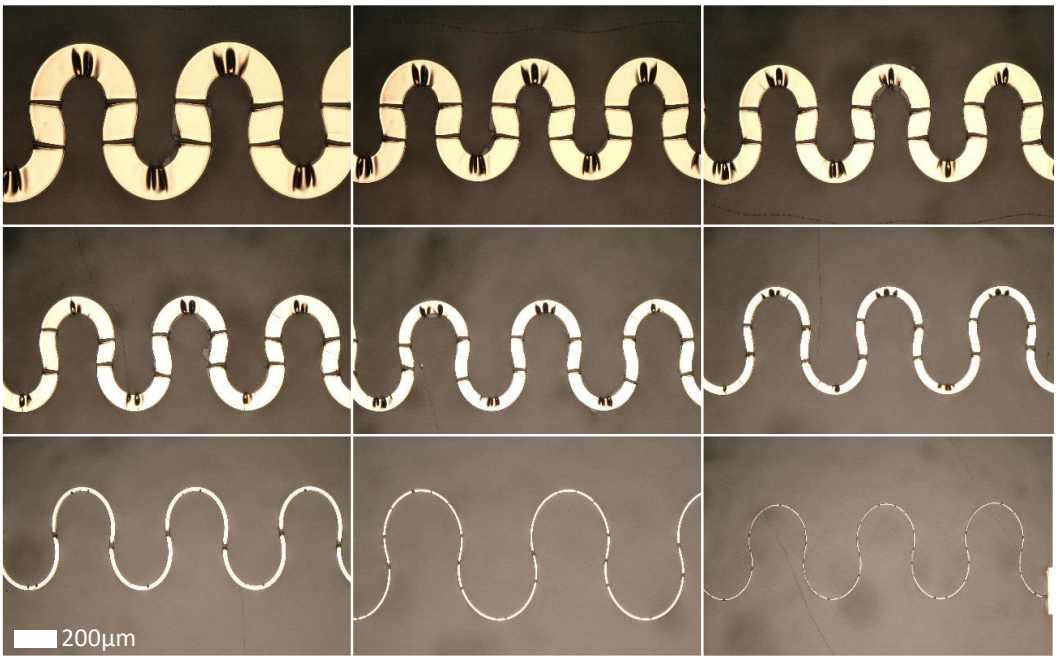

Supplementary Figure S6. Optical microscopy images showing horseshoe lines with different widths. These metallized/SU-8 lines on PDMS were fabricated using a photomask. Regular cracking is observed/

Supplementary Figure S6 shows the lithographically patterned horseshoe shaped lines. It was observed that these lines cracked at relatively low longitudinal strains (~5°). We observed that the cracking is relatively ordered, always occurring at the same places in the line. The cracking occurs as there is a large length of line in longitudinal direction of the applied strain. Contrast this to the transversally-orientated lines and the angled line study presented in the manuscript. The authors suggest that the 'amplitude' of such lines should be minimised whilst the period increased.

References

[1] Feng R and Farris R J 2003 Influence of processing conditions on the thermal and mechanical properties of SU8 negative photoresist coatings *J. Micromechanics Microengineering* **13** 80–8

[2] Robin C J, Vishnoi A and Jonnalagadda K N 2014 Mechanical Behavior and Anisotropy of Spin-Coated SU-8 Thin Films for MEMS *J. Microelectromechanical Syst.* **23** 168–80

[3] Dellmann L, Roth S, Beuret C, Racine G-A, Lorenz H, Despont M, Renaud P, Vettiger P and de Rooij N F 1998 Fabrication process of high aspect ratio elastic and SU-8 structures for piezoelectric motor applications *Sens. Actuators Phys.* **70** 42–7

[4] Mcaleavey A, Coles G, Edwards R L and Sharpe W N 1998 Mechanical properties of SU-8 *MRS Proceedings* vol 546

[5] Seghir R and Arscott S 2015 Extended PDMS stiffness range for flexible systems *Sens. Actuat A* **230** 33–9

[6] Lorenz H, Laudon M and Renaud P 1998 Mechanical characterization of a new high-aspect-ratio near UV-photoresist *Microelectron. Eng.* **41–42** 371–4